

Experimental study of the $^{56}\text{Ni}(^3\text{He},d)^{57}\text{Cu}$ reaction in inverse kinematics

C. L. Jiang, K. E. Rehm, D. Ackermann,^{*} I. Ahmad, J. P. Greene, B. Harss,[†] D. Henderson, W. F. Henning, R. V. F. Janssens, J. Nolen, R. C. Pardo, P. Reiter,[‡] J. P. Schiffer, D. Seweryniak, A. Sonzogni,[§] J. Uusitalo,^{||} I. Wiedenhöver,[¶] and A. H. Wuosmaa^{**}

Physics Division, Argonne National Laboratory, Argonne, Illinois 60439, USA

F. Brumwell and G. McMichael

IPNS, Argonne National Laboratory, Argonne, Illinois 60439, USA

M. Paul

Hebrew University, Jerusalem 90914, Israel

R. E. Segel

Physics Department, Northwestern University, Evanston, Illinois 60201, USA

(Received 30 July 2009; published 23 October 2009)

Measurements of $(^3\text{He},d)$ reactions can provide information on the proton widths of states that play a role in astrophysically important (p,γ) reactions. We report on the first study of the $(^3\text{He},d)$ reaction in inverse kinematics with a ^{56}Ni ($T_{1/2} = 6.1$ d) ion beam. The Q -value resolution of ~ 700 keV achieved in this experiment was sufficient to separate the transitions populating the ground state and the $1/2^-$ - $5/2^-$ doublet at $E_x \sim 1.1$ MeV in ^{57}Cu . Prospects for similar $(^3\text{He},d)$ experiments with improved energy resolution are also discussed.

DOI: [10.1103/PhysRevC.80.044613](https://doi.org/10.1103/PhysRevC.80.044613)

PACS number(s): 25.60.Je, 25.55.Hp, 27.40.+z, 29.38.Gj

I. INTRODUCTION

The nucleus ^{56}Ni with $N = Z = 28$, the heaviest easily accessible $N = Z$ doubly-magic nucleus, is of considerable interest, both for its structural properties and for its role in astrophysical processes. For nuclear structure, the energies and the degree of fragmentation of single-particle states provide important information for shell-model calculations. In nuclear astrophysics, the radiative capture of protons on medium-mass nuclei is an important reaction leading from lighter (CNO-cycle) nuclei to the mass 60–100 region. The long half-life of 6.1 d makes ^{56}Ni a critical waiting point nucleus in the astrophysical rapid proton (rp) capture process, because most of the reaction flow connecting the lighter ($A \leq 56$) nuclei with the heavier mass region passes through the $^{56}\text{Ni}(p,\gamma)^{57}\text{Cu}$ reaction [1].

There are many studies [2] of (p,γ) reactions on stable nuclei. The high proton intensities required to measure the small (typically μb) cross sections are readily available. In explosive nucleosynthesis, in hydrogen-rich environments

proton capture occurs on unstable nuclei, and different techniques for measuring these processes have to be employed. Capture reactions on unstable, but long-lived nuclides (e.g., ^7Be ($T_{1/2} = 53$ d) [3], ^{22}Na ($T_{1/2} = 2.6$ y) [4], and ^{26}Al ($T_{1/2} = 7.16 \times 10^5$ y) [5]) have been studied in the past. The high γ -ray background, however, makes these studies very challenging. Nuclei with shorter half-lives are only available as ion beams and, therefore, the only approach for a direct study of capture reactions is the use of inverse kinematics (i.e., bombarding a hydrogen target with a radioactive beam [6–9], and detecting either the γ rays in an efficient γ -detector array or the heavy reaction products in a high-acceptance mass separator). Despite the high efficiencies that can be achieved in experiments with inverse kinematics, the small cross sections still require beam intensities in excess of 10^8 particles/s, which are available so far only for a few, selected radioactive nuclei [6–8].

For other systems, indirect methods, such as Coulomb dissociation [10] or the asymptotic normalization coefficient (ANC) technique [11], are presently the only way to obtain information about the resonance strength $\omega\gamma$, defined as

$$\omega\gamma = \frac{(2J+1)\Gamma_p\Gamma_\gamma}{2(2j_t+1)\Gamma}, \quad (1)$$

where Γ_p , Γ_γ , and Γ are the proton, radiative, and total widths, and J and j_t are the spins of the resonance and the target nucleus, respectively. For the lowest energies (i.e., when $\Gamma_p \ll \Gamma_\gamma$) Eq. (1) reduces to

$$\omega\gamma = \frac{(2J+1)}{2(2j_t+1)}\Gamma_p. \quad (2)$$

^{*}Current address: GSI, D-64291 Darmstadt, Germany.

[†]Current address: Yazaki Europe Ltd., Cologne.

[‡]Current address: Institute of Nuclear Physics, University of Cologne, Germany.

[§]Current address: National Nuclear Data Center, Brookhaven National Laboratory, Upton, NY 11973, USA.

^{||}Current address: Department of Physics, University of Jyväskylä, Finland.

[¶]Current address: Physics Department, Florida State University, Tallahassee, FL 32306, USA.

^{**}Current address: Physics Department, Western Michigan University, Kalamazoo, MI 49008, USA.

The proton width Γ_p in Eq. (2) is related to the spectroscopic factor S through the equation

$$\Gamma_p = C^2 S \Gamma_p^{s.p.}, \quad (3)$$

where C^2 is the isospin Clebsch-Gordan coefficient for the state of interest ($=1$ for ^{56}Ni) and $\Gamma_p^{s.p.}$ is the proton single-particle width.

The spectroscopic factor is usually obtained through a comparison of the measured cross sections of a one-proton transfer [e.g., ($^3\text{He}, d$)] reaction to the distorted wave Born approximation (DWBA) prediction. In an earlier experiment [12], we have studied the neutron transfer reaction $^{56}\text{Ni}(d, p)^{57}\text{Ni}$ populating analog states in ^{57}Ni . In the present experiment we have measured angular distributions of the proton transfer reaction $^{56}\text{Ni}(^3\text{He}, d)^{57}\text{Cu}$ in inverse kinematics with a radioactive ^{56}Ni beam on a ^3He gas target.

II. EXPERIMENTAL DETAILS

The level structure of ^{57}Cu [13] is shown in Fig. 1. Because of the low (γ, p) threshold of 695 keV, only the $3/2^-$ ground state is particle-stable, while all excited states can decay via proton emission with half-lives that depend on their excitation energies, spin values and decay widths Γ_p and Γ_γ . Although no experimental values for these widths are available estimates based on the properties of the mirror states show [14] that the ratio Γ_γ/Γ_p for the first two excited states in ^{57}Cu at $E_x = 1.028$ and 1.106 MeV, respectively, is about 10^6 . Thus γ decay to the ground state in ^{57}Cu is the primary decay mode. For higher lying states the proton widths Γ_p increase exponentially, making proton decay to ^{56}Ni the dominant decay mode. In addition to the particle-stable $3/2^-$ ground state, one therefore expects in a deuteron- ^{57}Cu coincidence experiment only events from the population of the $5/2^-$ - $1/2^-$ doublet at 1.028 and 1.106 MeV, respectively, which, because of their close proximity cannot be separated.

The requirement of “inverse kinematics” puts additional constraints on the experiment. At bombarding energies of 4–5 MeV/u, the maxima of the angular distributions from which the spectroscopic factor is obtained, are typically in the $\theta_{\text{cm}} = 20^\circ$ – 70° range. In Fig. 2(a), we present the kinematic curves for the $^3\text{He}(^{56}\text{Ni}, d)^{57}\text{Cu}$ reaction. Since the outgoing deuterons have to be energetic enough to penetrate the exit foil of the ^3He gas cell (typically 2–3 MeV), only the cm region with $\theta_{\text{cm}} \geq 30^\circ$ is accessible. The strong kinematic shift $dE/d\theta$ of about 500 keV/ $^\circ$ restricts the Q -value resolution that can be achieved. An advantage of the inverse kinematics

$5/2^-$	—————	2.398
$1/2^-$	=====	1.106
$5/2^-$	- - - - -	1.028
		0.695
$3/2^-$	—————	0.0

^{57}Cu

FIG. 1. Level structure of ^{57}Cu . The dashed line represents the (γ, p) threshold in ^{57}Cu .

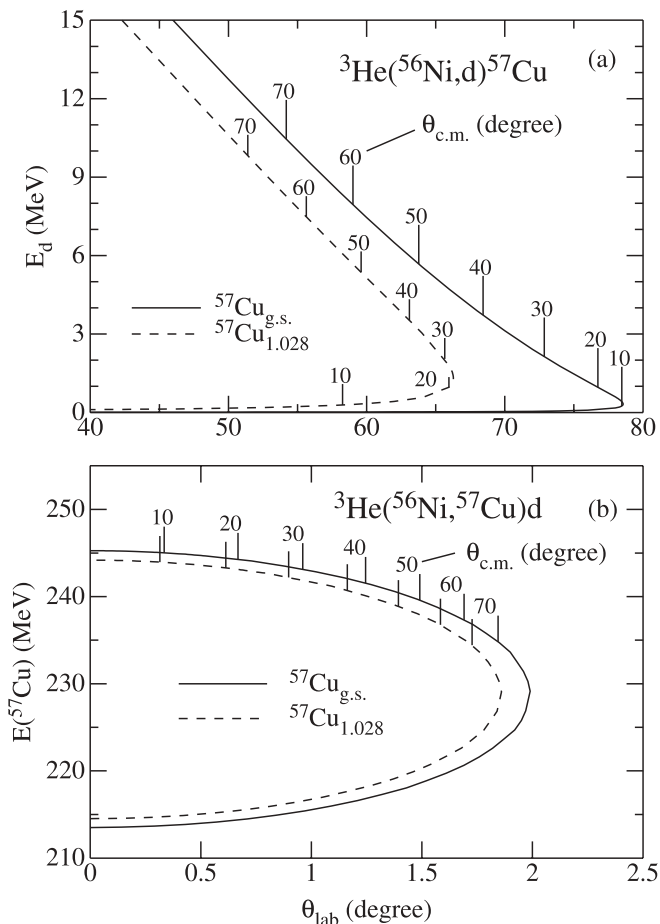
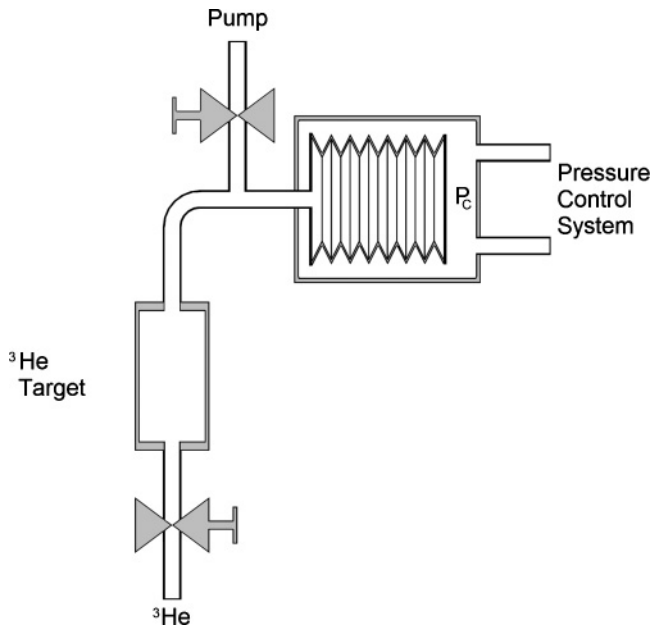


FIG. 2. (a) Kinematics for the $^3\text{He}(^{56}\text{Ni}, d)^{57}\text{Cu}$ reaction, populating the ground (solid line) and excited $5/2^-$ state (dashed line) in ^{57}Cu at an incident energy of 250 MeV. The vertical lines mark the center-of-mass angles. (b) Kinematic curves of the outgoing ^{57}Cu reaction products.

is the small transverse momentum of the emitted deuterons. This restricts the ^{57}Cu recoil particle to angles smaller than 2° , well within the acceptance limits of the FMA [see Fig. 2(b)].

The radioactive ^{56}Ni material was produced via the $^{58}\text{Ni}(p, p2n)^{56}\text{Ni}$ reaction with a 50-MeV proton beam from the injector of the Intense Pulsed Neutron Source (IPNS) at Argonne. The irradiated material was inserted into the negative ion source of the ATLAS accelerator and the ^{56}Ni ions were accelerated to an energy of 290 MeV using the superconducting heavy-ion accelerator. Details of the beam production and monitoring techniques are given in Refs. [12,15].

After acceleration, the ^{56}Ni beam hits a gas target, schematically shown in Fig. 3. It consists of a ~ 2 -mm-long, 10-mm-diameter, cylindrical ^3He gas cell, which is cooled to liquid nitrogen temperatures, to increase the ^3He density. The entrance and exit foils of the target consist of 1.9 mg/cm 2 thick HAVAR foils. The length of the pressurized target was measured with a micrometer to be 2.1 mm. At a temperature of 89 K and a pressure of 700 mbar, the total target thickness is 65 $\mu\text{g}/\text{cm}^2$ or 1.35×10^{19} particles/cm 2 . At a bombarding energy of 290 MeV, the ^{56}Ni energy in the middle of the target is calculated to be 250 MeV. To keep the helium pressure constant

FIG. 3. Schematic of the ^3He gas-cell target.

(i.e., to compensate for the diffusion of helium through the gas cell windows) the target volume is connected to a ^3He reservoir consisting of a 15-cm-long, 10-cm-diameter bellows. A pressure control system kept the pressure outside the bellows and, thus, also inside the gas cell, constant to better than 0.5%.

The outgoing deuterons were detected in a barrel-shaped, position-sensitive detector array, which is shown schematically in Fig. 4. It consisted of six 5×5 cm² Si strip detectors (with a strip width of 2 mm) arranged as a hexagon in the forward direction, covering the angular range $\theta_{\text{lab}} = 45^\circ$ – 76° and corresponding to a solid angle of about 2.7 sr. The 6×25 strips were read out individually using amplifiers developed at Argonne.

Because the incident ^{56}Ni beam had a considerable contamination from the isobars ^{56}Co and ^{56}Fe , the deuterons detected in the Si strip detector array were measured in

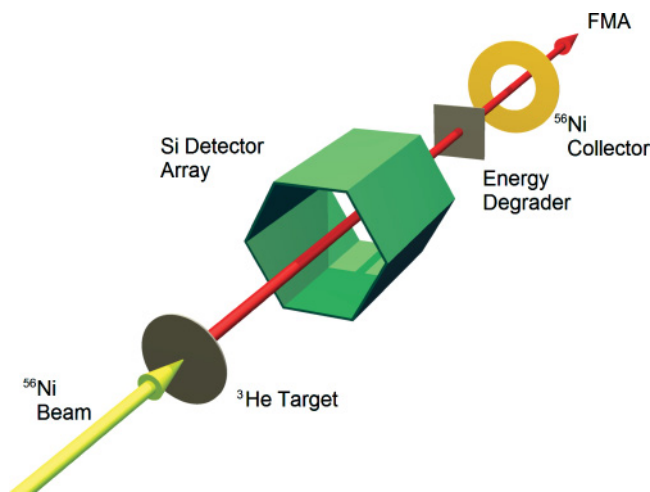


FIG. 4. (Color online) Schematic of the experimental setup.

coincidence with the (energy-degraded) heavy residual nuclei ^{57}Cu , ^{57}Ni , or ^{57}Co , which were identified with respect to mass and nuclear charge in the focal plane of the FMA (see Ref. [15] for details). Charge state distributions were measured with ^{56}Ni , ^{56}Co , and ^{56}Fe beams, and the results were then extrapolated to ^{57}Cu , for which no experimental data are available. From these measurements, the maximum of the ^{57}Cu charge state distribution is predicted to be at $q = 22^+$. The choice of $^{57}\text{Cu}^{23+}$ for the FMA setting resulted in an additional suppression of the ^{57}Ni and ^{57}Co contaminants. Under these experimental conditions, the count rate for a cross section of 1 mb/sr and a beam intensity of 5×10^4 particles/s was about 3 counts/h.

An important issue for $(^3\text{He},d)$ reactions measured in inverse kinematics is the Q -value resolution that can be achieved. For the one-neutron transfer reaction $d(^{56}\text{Ni},p)^{57}\text{Ni}$ discussed in Ref. [15], a Q -value resolution of ~ 300 keV was achieved. One of the differences between (d,p) and $(^3\text{He},d)$ reactions studied in inverse kinematics is the compression of the kinematic curves. In the $d(^{56}\text{Ni},p)^{57}\text{Ni}$ reaction at energies of 4–5 MeV/u, the critical angle region in the laboratory is between 120° and 160° . Owing to the compression of the kinematic curves, protons populating two states separated by 1 MeV in excitation energy differ in their laboratory energies by only 500 keV. This complicates the separation of closely spaced states in the final nucleus.

For the inverse $^3\text{He}(^{56}\text{Ni},d)^{57}\text{Cu}$ reaction, the critical angle region is between laboratory angles of 45° and 70° . For this kinematics, deuterons populating states separated by 1 MeV in excitation energy differ by about 2 MeV in the laboratory system [see Fig. 2(a)]. This advantage, however, is more than compensated by other effects, which, taken together, make $(^3\text{He},d)$ studies in inverse kinematics very challenging. The main difference between (d,p) and $(^3\text{He},d)$ reactions influencing the Q -value resolution is in the kinematic shift. Whereas for the $d(^{56}\text{Ni},p)^{57}\text{Ni}$ reaction the kinematic shift $dE/d\theta$ is between 30 and 80 keV/ $^\circ$, the kinematics of the $^3\text{He}(^{56}\text{Ni},d)^{57}\text{Cu}$ reaction has $dE/d\theta$ values of 400–600 keV/ $^\circ$. This places severe constraints on the angle determination of the outgoing particles.

To simulate the various contributions to the Q -value resolution, we developed a Monte Carlo program that takes the intrinsic energy resolution (50 keV), the detector geometry, and the beam-spot size as well as energy and small-angle scattering in the gas target into account. Results from these simulations are presented in Fig. 5. The scatter plot in the top part represents the influence of the gas target on the kinematic curves for deuterons from the $^3\text{He}(^{56}\text{Ni},d)^{57}\text{Cu}$ reaction populating the first two states in ^{57}Cu . Converting the scatter plot into Q -value spectra results in the one-dimensional plot of Fig. 5(b). The full width at half maximum of this spectrum, which represents the influence of the gas target, is ~ 200 keV. Including the geometry of the Si array (i.e., the detector strip size of 2 mm, a beam spot diameter of 2 mm, and the length of the target of 2 mm) deteriorates the Q -value resolution to about 400 keV, as shown by the dotted line in Fig. 5(c). A 1-mm displacement of the beam spot on the target deteriorates the Q -value resolution to about 600 keV, as shown by the solid line in Fig. 5(c). This value is close to the experimental result

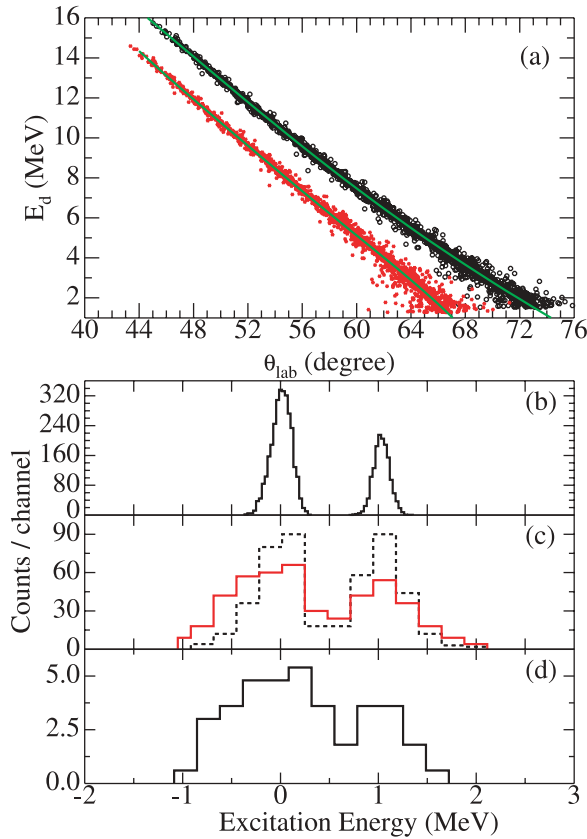


FIG. 5. (Color online) (a) Results of Monte Carlo simulations for the energy-angle correlation of the outgoing deuterons from the ${}^3\text{He}$ gas cell for the ground and first excited state of ${}^{57}\text{Cu}$, respectively. The solid lines are the results without angular and energy straggling effects in the foils and the ${}^3\text{He}$ gas. (b), (c) Monte Carlo simulation of the excitation energy spectra for the ${}^3\text{He}({}^{56}\text{Ni},d){}^{57}\text{Cu}$ reaction taking detector and target effects into account. (d) Experimental spectrum. See text for details.

($\Delta Q \sim 700$ keV), which is given in Fig. 5(d). This resolution is sufficient to separate the ground state from the first two excited states in ${}^{57}\text{Cu}$.

III. EXPERIMENTAL RESULTS

From the experimental Q -value spectrum in Fig. 5(d), angular distributions for the $3/2^-$ state and the $1/2^-$ - $5/2^-$ doublet in ${}^{57}\text{Cu}$ were obtained (see Fig. 6). Because of low counting statistics and the slowly varying cross sections, the data were binned into six and seven angle ranges. The acceptance of the FMA was estimated using a Monte Carlo calculation [16], taking the charge-state efficiency into account. The maximum cross sections are a few mb/sr in the angular range $\theta_{\text{cm}} \sim 40^\circ$ - 70° . The uncertainties are dominated by counting statistics.

For the $({}^3\text{He},d)$ reaction, the experimental cross section $(\frac{d\sigma}{d\Omega})_{\text{exp}}$ is related to the cross section predicted by the DWBA through the equation

$$\left(\frac{d\sigma}{d\Omega}\right)_{\text{exp}} = C^2 S_p \times C^2 S_t \left(\frac{d\sigma}{d\Omega}\right)_{\text{DWBA}}, \quad (4)$$

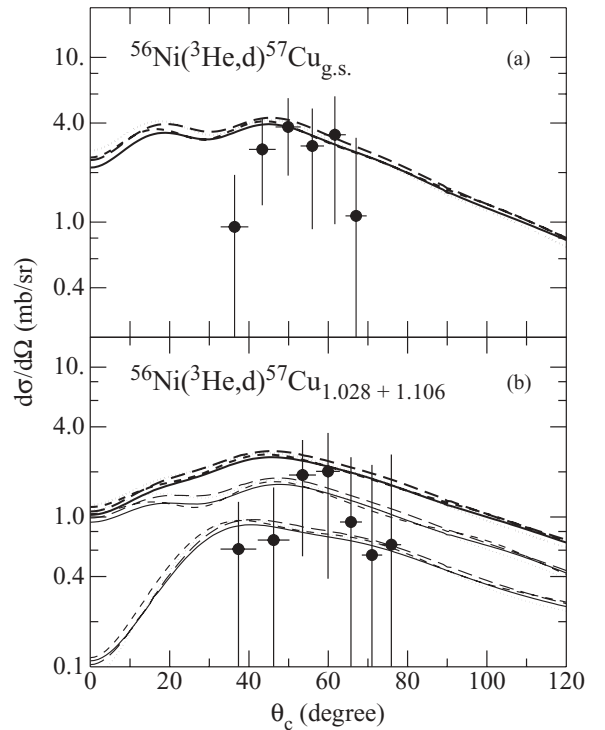


FIG. 6. Experimental angular distributions and comparisons with DWBA calculations; (a) $3/2^-$ ground state. (b) $1/2^-$ and $5/2^-$ states at $E_x = 1.106$ MeV and 1.028 MeV (upper and lower thin lines), respectively. The thick lines give the summed cross section.

where C and S are the isospin Clebsch-Gordan coupling coefficients and spectroscopic factors of the transferred particle in the projectile and target nucleus, respectively.

The DWBA calculations were carried out with the full finite range code PTOLEMY [17]. There are many sets of optical potential parameters available in the literature for $({}^3\text{He},d)$ reactions at energies of 5–10 MeV/u. Because of the large uncertainties in the data, we have used only a few selected sets [18–20]. For the projectile, the results from a calculation using realistic wave functions for ${}^3\text{He}$ and d ($C^2 S_p = 1.3$) [21] were used.

The results of the calculations are indicated by the curves in Fig. 6 and the potential parameters are listed in Table I. From a comparison of the data with the DWBA calculations, spectroscopic factors $C^2 S_t$ of 0.6 and 0.75 for the $3/2^-$, $5/2^-$, and $1/2^-$ states in ${}^{57}\text{Cu}$ were obtained. Because of the limited statistics the uncertainties are about 40%. These values are in good agreement with single-particle expectations, if one considers that short-range correlations lead to a quenching of the spectroscopic factors. Similar effects have been observed for electromagnetic properties [$B(E2)$ values and magnetic moments] of nuclei around ${}^{56}\text{Ni}$ [22,23].

In this first $({}^3\text{He},d)$ experiment in inverse kinematics, the statistics were limited by the intensities presently available for a radioactive ${}^{56}\text{Ni}$ beam, but the comparison between experiment and DWBA calculation confirms our earlier conclusion [12] that the low-lying states in ${}^{57}\text{Cu}$ are good single-particle states. As a result, the astrophysical rate of

TABLE I. Optical model parameters used in the DWBA calculations.^a

Potential	Particle	V (MeV)	r_0 (fm)	a (fm)	W (MeV)	W' (MeV)	r'_0 (fm)	a' (fm)	V_{so} (MeV)	r_{0c} (fm)
Set A ^b	^3He	177.8	1.14	0.723	25.72	0	1.548	0.80	0	1.40
	d	112.0	0.974	0.912	0	18.3	1.439	0.60	6	1.30
Set B ^b	^3He	139.0	1.08	0.80	12.3	0	1.743	0.721	0	1.40
	d	89.8	1.15	0.81	0	18.4	1.34	0.68	0	1.30
Set C ^c	^3He	174.5	1.07	0.85	13.5	0	1.81	0.59	0	1.40
	d	112.0	1.0	0.9	0	18.0	1.55	0.47	6	1.30
Set D ^d	^3He	149.4	1.08	0.77	18.0	0	1.63	0.76	0	1.25
	d	101.0	1.06	0.85	0	19.5	1.33	0.68	0	1.25

^aThe potentials for ^3He and d were of the form $V(r) = -V[1 + \exp(x)]^{-1} - i[W - 4W'(d/dx)]/[1 + \exp(x)]^{-1} + 4V_{\text{so}}(1/r)(d/dr)[1 + \exp(x)]^{-1}(L \cdot S) + V_c(r, r_c)$ with $x = (r - r_0A^{1/3})/a$, $x' = (r - r'_0A^{1/3})/a'$, and $r_c = r_{0c}A^{1/3}$.

^bRef. [18].

^cRef. [19].

^dRef. [20].

the $^{56}\text{Ni}(p,\gamma)^{57}\text{Cu}$ reaction is larger than earlier theoretical estimates by more than an order of magnitude (see Ref. [12]).

Improvements in statistics for this experiment are difficult. The target thickness and the solid angle coverage of the Si array can be increased only slightly. The overall detection efficiency is dominated by the charge-state fraction of the outgoing $^{57}\text{Cu}^{23+}$ recoils ($\sim 20\%$). The use of the FMA for recoil detection could be avoided if a pure beam of ^{56}Ni became available. However, since the ^{56}Ni - ^{56}Co mass difference is small (only 2293 μu), a mass separator with very high resolution ($M/\Delta M \geq 2.5 \times 10^4$) would be required to produce an isotopically pure ^{56}Ni beam. For this reason, the only realistic possibility to improve the statistics in this experiment is a higher intensity ^{56}Ni beam.

IV. OUTLOOK AND CONCLUSION

The nucleus studied in this experiment is an important waiting point in the astrophysical rp process. It is also experimentally accessible, owing to the low level density in the vicinity of the ground state of ^{57}Cu . From the spectroscopic factors measured in neutron and proton transfer reactions, the astrophysical reaction rate for the $^{56}\text{Ni}(p,\gamma)^{57}\text{Cu}$ reaction is larger than predicted by previous theoretical estimates.

There are many other (p,γ) reactions, populating higher excited states, where a considerable increase in Q -value resolution is required to separate the states of interest. For this reason it is interesting to investigate where improvements in the Q -value resolution can be made. In Fig. 7(a), the individual contributions to the Q -value resolution are shown, plotted as function of the laboratory angle. Curve A represents the effects of small-angle straggling in the entrance and exit foils of the gas target. Curve B provides the corresponding effects of energy straggling. The size of the strip detector and its geometry results in curve C. In curve D, a 2-mm beam spot is included in the geometry, whereas in curve E a possible shift of the beam spot by 1 mm is included as well. All contributions, added in quadrature, result in curve F. As can be seen, the Q -value resolution is dominated by contributions

from the geometry of the detector: pixel size, beam spot diameter, and alignment of the beam spot with respect to the axis of the detector array. Small-angle straggling of the outgoing deuterons increases its importance at larger angles. As can be seen from curve F, a total Q -value resolution of about 600 keV is obtained in the present setup. From Fig. 7 it can also be seen how the Q -value resolution can be improved: Increasing the distance from target to detector (i.e., doubling the diameter and the length of the Si-detector array) leads to an improvement of the geometry, resulting in an Q -value resolution of 250 keV. The effect of small-angle straggling can further be reduced by replacing the exit foil of the gas target with one made of lower Z material (e.g., Kapton).

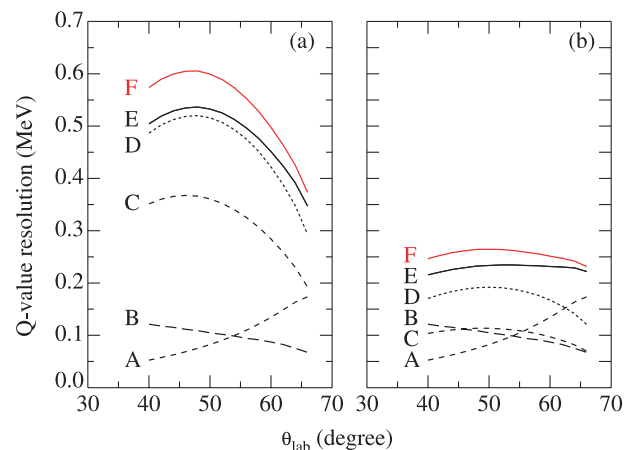


FIG. 7. (Color online) (a) Contributions to the Q -value resolution of the deuteron spectrum in the present experiment: A, angular straggling in the gas cell foils; B, energy straggling in the foils; C, effects of the detector geometry; D, geometry and effects of the beam spot size at the ^3He gas target; E, geometry, beam spot size and effect of a shift of the beam position by 1 mm. The line F gives the sum of all contributions added in quadrature. (b) Q -value resolutions obtained by increasing the distance between target and detector by a factor of 2.

More recently, a new type of spectrometer, optimized for the study of reactions in inverse kinematics, has been proposed and a prototype has been constructed [24]. It consists of a cylindrical magnet with a strong axial field. In this spectrometer, the outgoing particles move on helical trajectories and are detected in a position-sensitive detector array surrounding the axis of the spectrometer. Simulating the Q -value resolution of such a device for the ${}^3\text{He}({}^{56}\text{Ni}, d){}^{57}\text{Cu}$ reaction results in a value of $\Delta Q \sim 150$ keV, making this

spectrometer an excellent tool for $({}^3\text{He}, d)$ studies in inverse kinematics.

ACKNOWLEDGMENTS

This work was supported by the US Department of Energy, Office of Nuclear Physics, under Contract No. DE-AC02-06CH11357 (ANL) and DE-FG02-98ER-41086 (NWU).

-
- [1] H. Schatz *et al.*, Phys. Rep. **294**, 167 (1998).
 - [2] C. Rolfs and C. A. Barnes, Annu. Rev. Nucl. Part. Sci. **40**, 45 (1990).
 - [3] B. W. Filippone, A. J. Elwyn, C. N. Davids, and D. D. Koetke, Phys. Rev. Lett. **50**, 412 (1983); A. R. Junghans *et al.*, Phys. Rev. C **68**, 065803 (2003).
 - [4] J. Görres *et al.*, Phys. Rev. C **39**, 8 (1989); F. Stegmüller *et al.*, Nucl. Phys. **A601**, 168 (1996).
 - [5] R. B. Vogelaar, Ph.D. thesis, California Institute of Technology, 1989.
 - [6] P. Decrock *et al.*, Phys. Rev. Lett. **67**, 808 (1991).
 - [7] S. Bishop *et al.*, Phys. Rev. Lett. **90**, 162501 (2003); **90**, 229902(E) (2003).
 - [8] C. Ruiz *et al.*, Phys. Rev. Lett. **96**, 252501 (2006).
 - [9] K. E. Rehm *et al.*, Nucl. Instrum. Methods Phys. Res. A **418**, 355 (1998).
 - [10] G. Baur and H. Rebel, Annu. Rev. Nucl. Part. Sci. **46**, 321 (1996).
 - [11] A. M. Mukhamedzanov, C. A. Gagliardi, and R. E. Tribble, Phys. Rev. C **63**, 024612 (2001).
 - [12] K. E. Rehm *et al.*, Phys. Rev. Lett. **80**, 676 (1998).
 - [13] X. G. Zhou, H. Dejbakhsh, C. A. Gagliardi, J. Jiang, L. Trache, and R. E. Tribble, Phys. Rev. C **53**, 982 (1996).
 - [14] J. M. Blatt and V. E. Weisskopf, *Theoretical Nuclear Physics* (Wiley, New York, 1962).
 - [15] K. E. Rehm *et al.*, Nucl. Instrum. Methods Phys. Res. A **449**, 208 (2000).
 - [16] C. L. Jiang and C. N. Davids, ANL Physics Division Annual Report ANL-95/14, p. 74, 1995.
 - [17] M. H. MacFarlane and S. C. Pieper, Argonne National Laboratory Report No. ANL-76-11 (Rev.1), 1978 (unpublished).
 - [18] D. J. Pullen, B. Rosner, and O. Hansen, Phys. Rev. **166**, 1142 (1968).
 - [19] B. Cujec and I. M. Szöghy, Phys. Rev. **179**, 1060 (1969).
 - [20] B. Zeidman, R. H. Siemssen, G. C. Morrison, and L. L. Lee Jr., Phys. Rev. C **9**, 409 (1974).
 - [21] R. Schiavilla, V. R. Pandharipande, and R. B. Wiringa, Nucl. Phys. **A449**, 219 (1986); R. B. Wiringa (private communication).
 - [22] S. Raman, C. W. Nestor Jr., and P. Tikannen, At. Data Nucl. Data Tables **78**, 1 (2001).
 - [23] K. Minamisono *et al.*, Phys. Rev. Lett. **96**, 102501 (2006).
 - [24] A. H. Wuosmaa *et al.* Nucl. Instrum. Methods Phys. Res. A **570**, 536 (2007).